GRAVITATIONAL LENSING STATISTICS AND CONSTRAINTS ON THE COSMOLOGICAL CONSTANT REVISITED

Yu-Chung N. Cheng¹ and Lawrence M. Krauss²

Department of Physics, Case Western Reserve University, Cleveland, OH 44106-7079

We re-analyze constraints on the cosmological constant that can be obtained by examining the statistics of strong gravitational lensing of distant quasars by intervening galaxies, focusing on uncertainties in galaxy models (including velocity dispersion, luminosity functions, core radii and magnification bias effects) and on the parameters of the galaxy distribution and luminosity functions. In the process we derive new results on magnification biasing for galaxy lenses with nonzero core radii, and on how to infer the proper velocity dispersions appropriate for use in lensing statistics. We argue that the existing data do not disfavor a large cosmological constant. In fact, for a set of reasonable parameter choices, using the results of 5 optical quasar lensing surveys we find that a maximum likelihood analysis favors a value of Ω_0 in the range ≈ 0.25 -0.55 in a flat universe. An open cosmology is not favored by the same statistical analysis. Systematic uncertainties are likely to be dominant, however, as these results are sensitive to uncertainties in our understanding of galaxy luminosity functions, and dark matter velocity dispersions, as well as the choice of lensing survey, and to a lesser extent the existence of core radii. Further observational work will be required before it is possible to definitively distinguish between cosmological models on the basis of gravitational lensing statistics.

1 Introduction

Recently there has been a renewed interest in the possibility that the cosmological constant may dominate the energy density of the universe, in order to resolve several cosmological conundra [1, 2, 3], and more recently due to direct observational measurements of the distance redshift relation [4, 5]. For some time, one of the few cosmological pieces of evidence which has appeared apparently disfavoring this possibility has involved analyses of the statistics of gravitational lensing of quasars by galaxies [6, 7, 8, 9].

The effort to constrain cosmological parameters utilizing such statistics is of course highly dependent both on the quality of the existing data, and also on the robustness of the theoretical inputs in the analysis. Because of the potential importance of the claimed constraints on a cosmological constant, it is worth re-examining in some depth the dependence of the resulting constraints on model dependent assumptions, as well as making some attempt to improve the models of galaxies one uses in the analysis.

¹E-mail address: vxc16@po.cwru.edu

²Also Dept. of Astronomy, E-mail address: krauss@theory1.phys.cwru.edu

In this paper, we re-analyze lensing statistics, concentrating on the role of the luminous E/S0 galaxy distribution function and luminosity function parameters, and the self consistent modelling of galaxy parameters, including core radii. As we shall show, new considerations of the velocity dispersions of lensing galaxies [8, 10], the core radii of lensing galaxies [7, 11], and the magnification bias resulting from selection effects [8, 9, 11, 12] both affect the nature of the constraints one derives, and also imply that the constraints presently possible from the statistics of strong lensing may vary over a wide range. Nevertheless, we find for reasonable parameters, a best fit cosmology with a low matter density flat universe with a cosmological constant [13]³. Moreover, we find that the data that favors a low Ω_0 mildly favors a flat cosmological constant dominated universe over an open universe. Five sets of quasar surveys are considered in order to compare predictions and observations.

2 Theory layout: core radii, magnification bias, lensing statistics, and galaxy parameters

In this section we first review the basic formalism we shall utilize in our statistical analyses, including the calculation of optical depths for lenses modelled as isothermal spheres with core radii. We then proceed to a new calculation of the relevant magnification bias which should be utilized in this situation. This is significant, because the trade off between reduction in lensing probability caused by finite cores is offset to some degree by an increase in the magnification bias due to lensing [9]. The degree of this offset is important, however, if the two effects do not precisely cancel, as we find. We conclude this section with a short summary of our statistical maximum likelihood method.

2.1 Optical depths and nonsingular isothermal spheres

We begin by modelling the mass density distribution of elliptical galaxies with the following form [11]:

$$\rho(r) = \frac{\sigma_{\rm DM}^2}{2\pi G(r^2 + r_{\rm c}^2)} \tag{1}$$

where $\sigma_{\rm DM}$ is the velocity dispersion of this system (presumably the dominant dark matter, a consideration we shall return to later), and $r_{\rm c}$ is the core radius. When $r_{\rm c}$ is zero, this model reverts to a singular isothermal sphere (SIS) model. With the density distribution from equation (1), one can calculate the lensing cross section, $\sigma_{\rm cs}$, within which multiple images of gravitational lensing events are observed.

$$\sigma_{\rm cs} = \pi a_{\rm cr}^2 f(\beta) \tag{2}$$

where

$$a_{\rm cr} = \frac{c \alpha_0 y_{o\ell} y_{\ell s}}{H_o(1 + z_\ell) y_{os}} \tag{3}$$

³As this paper was being finalized for submission a new investigation [14] also appeared which explores several similar issues and reaches compatible conclusions.

 $a_{\rm cr}$ is the critical radius, z is the redshift, and $\alpha_0 = 4\pi (\frac{\sigma_{\rm DM}}{c})^2$, is the bend angle for an isothermal sphere with core radius $r_{\rm c} = 0$. The Hubble constant H_o is 100 h km s⁻¹ Mpc⁻¹. (Please note that this $a_{\rm cr}$ was the size at lens redshift z_l . It is not the critical radius at the present Universe.) The y quantities are angular diameter distances between the source, lens and observer, and will be discussed in more detail below. The quantity, $\beta \equiv r_{\rm c}/a_{\rm cr}$ as defined in Hinshaw & Krauss [11], and

$$f(\beta) \equiv 1 + 5\beta - \frac{1}{2}\beta^2 - \frac{1}{2}\sqrt{\beta}(\beta + 4)^{\frac{3}{2}}$$
 (4)

These quantities arise in the determination of the bend angle, α , of the light trace from the source, which in the case of an isothermal sphere with a finite core radius, is a function of the velocity dispersion $\sigma_{\rm DM}$, impact parameter b, and core radius $r_{\rm c}$ [11]. The general formula for the bend angle is:

$$\alpha(b) = \frac{4b}{c^2} \int_b^\infty dr \frac{\partial \Phi}{\partial r} \frac{1}{\sqrt{r^2 - b^2}}$$
 (5)

where

$$\Phi(\vec{r}) = -\int_{v} d^{3}\vec{r'} \frac{G\rho(\vec{r'})}{|\vec{r} - \vec{r'}|}$$

$$\tag{6}$$

After calculating bend angles of multi images, one can then calculate the image separation, $\Delta\theta$, and compare to measurements.

The full lensing probability can then also be calculated as follows:

$$\tau = \int d\tau = \int_0^{z_s} dz_l \int_0^\infty d\left(\frac{L}{L^*}\right) \left(\frac{y_{ol}y_{ls}}{y_{os}}\right)^2 \frac{FB(\langle m)f(\beta)}{\sqrt{\Omega_o(1+z_l)^3 + \Omega_R(1+z_l)^2 + \Omega_\Lambda}} \left(\frac{L}{L^*}\right)^\alpha \exp\left(-\frac{L}{L^*}\right)$$
(7)

where

$$F = \frac{c^3 \pi n \alpha_0^2}{\mathrm{H_o}^3}.$$
 (8)

The galaxy number density n is the luminous E/S0 galaxy density, which is about 30 per cent of the total galaxy number density [15], which is taken to be is $1.40 \times 10^{-2} h^3$ Mpc⁻³, given by Loveday et al. [16]. Spiral galaxies are not important in studies of strong lensing, because of their huge core radii [7]. $\Omega_{\rm R}$ is the curvature term, and Ω_{Λ} is the cosmological constant, so that $\Omega_{\rm o} + \Omega_{\rm R} + \Omega_{\Lambda} = 1$ in all cases. In a flat universe, y_{ls} is simply y_{os} - y_{ol} . However, in an open universe (with $\Omega_{\Lambda} = 0$):

$$y_{ls} = y_{os} \sqrt{1 + \Omega_{\rm R} y_{ol}^2} - y_{ol} \sqrt{1 + \Omega_{\rm R} y_{os}^2}$$
 (9)

 y_{oi} is the angular size distance [17]:

$$y_{oi} \equiv \frac{1}{\sqrt{\Omega_{\rm R}}} \sinh\left(\sqrt{\Omega_{\rm R}} \int_0^{z_i} \frac{dz}{\sqrt{\Omega_{\rm o}(1+z)^3 + \Omega_{\rm R}(1+z)^2 + \Omega_{\Lambda}}}\right)$$
(10)

B(< m) is the magnification bias factor, which takes into account that lensed quasars are magnified, and thus have a larger probability of being observed than unlensed quasars, as we

shall discuss in the next section. We also have to integrate the lensing probability density over the lens luminosity distribution L, which is assumed to be given by the Schechter luminosity function [18]:

$$\phi(L)dL = \left(\frac{L}{L^*}\right)^{\alpha} \exp\left(-\frac{L}{L^*}\right) d\left(\frac{L}{L^*}\right) \tag{11}$$

The parameters of the Schechter function will be discussed in some detail later, as they induce perhaps the dominant uncertainties in the predictions for the gravitational lensing of quasars by galaxies.

2.2 Magnification bias

Magnification bias in a lensing analysis is due to the amplification of lensed quasar images. Because of this effect, an observer can observe a lensing event which cannot be seen if either it is not lensed or its magnification factor is not large enough to raise it above the minimum sensitivity of a flux-limited survey. A magnification bias factor, which enhances the optical depth compared to the bare optical depth calculated in the absence of this selection effect, can be estimated based on flux limits and the presumed luminosity distribution of quasars. This factor has been estimated earlier to be as large as 26 in the case of initial lensing surveys using a singular isothermal sphere (SIS) model for galaxy lenses [12]. Its formula and its value have been re-examined by Fukugita & Turner [6], and the value can be as low as 4, if the survey of a complete set of quasars with apparent magnitude less than 22 can be achieved. Amplification of a lensed quasar including a core radius of the lensing galaxy has been discussed in Hinshaw & Krauss [11]. However, the bias factor has not been calculated before for this case. Here we carry out such an analysis.

We begin with the definition of amplification (A) of a lensed quasar and also include the core radius in our formulas. Following Peebles [17],

$$A = \left| \frac{\theta d\theta}{\theta_{\mathcal{Q}} d\theta_{\mathcal{Q}}} \right| = \left| \frac{b db}{\ell d\ell} \right| = \left| \frac{x dx}{L_1 dL_1} \right| \tag{12}$$

where θ is the angle between the lens and the pseudo image of the quasar, $\theta_{\rm Q}$ is the angle between the lens and the real quasar, b is the impact parameter, ℓ is the transverse (projected) distance of the lens center from the line of sight, and $x \equiv b/a_{\rm cr}$, $L_1 \equiv \ell/a_{\rm cr}$. We will see that the amplification A is a function of L_1 and β only, as discussed below. Following equation (6) in Hinshaw & Krauss [11], $0 \le L_1 \le L_0 \equiv \frac{\ell_0}{a_{\rm cr}} \le 1$, and $0 \le \beta \le \frac{1}{2}$, we can easily rewrite that equation to be

$$L_1 = -x + \frac{\sqrt{x^2 + \beta^2} - \beta}{x} \tag{13}$$

This means that although A is a function of L_1 , x, and β , we can rewrite A in terms of L_1 and β only. Using equation (13), we have

$$\frac{dL_1}{dx} = \frac{1}{\sqrt{x^2 + \beta^2}} - \frac{L_1}{x} - 2\tag{14}$$

and we can calculate the amplification A. For the total amplification, we sum up the absolute values of amplification caused by each individual image, i.e.,

$$A = \sum_{i} \left| \frac{x_i dx_i}{L_1 dL_1} \right| \tag{15}$$

where x_i are the solutions of equation (13), shown in Cheng & Krauss [19]. With

$$\ell_0^2 \equiv a_{\rm cr}^2 + 5a_{\rm cr}r_{\rm c} - \frac{1}{2}r_{\rm c}^2 - \frac{1}{2}r_{\rm c}^{1/2}(r_{\rm c} + 4a_{\rm cr})^{3/2}$$
(16)

(we should remind our readers that L_o^2 is actually identical to equation (4) above.) we can define the averaged amplification as a function of β :

$$\langle A \rangle \equiv \frac{\int_0^{L_o} dL_1 L_1 A(L_1, \beta)}{\int_0^{L_o} dL_1 L_1} = \frac{2}{L_o^2} \int_0^{L_o} dL_1 L_1 A(L_1, \beta)$$
 (17)

The numerical values of $\langle A \rangle$ are listed in Table 1.

Our next step is to calculate the minimum value of amplification $(A_{\rm M})$ from the three quasar images for a given β , which will be used in the magnification bias calculation. The numerical results are listed in Table 2. The values of β , the corresponding minimum values of amplification, the corresponding L_1 values at $A_{\rm M}$, and the corresponding L_0 are listed in Table 2. We have also found that $A_{\rm M}$ can be well fitted by $2/(L_0^{0.65})$ and plotted in Figure 1. We will use this approximation in our magnification bias calculation.

We can now derive the magnification bias. We start with the probability density of amplification

$$p(A)dA = 2A_{\mathcal{M}}^2 A^{-3} dA, \qquad A \ge A_{\mathcal{M}}$$

$$\tag{18}$$

such that

$$\int_{A_{\mathcal{M}}}^{\infty} p(A)dA = 1 \tag{19}$$

If we define

$$\Delta \equiv 2.5 \log_{10} A$$

$$\Delta_{\min} \equiv 2.5 \log_{10} A_{M}$$
(20)

then we have

$$p(A)dA = p(\Delta)d\Delta = 0.8(\ln 10)A_{\rm M}^2 10^{-0.8\Delta} d\Delta$$
 (21)

The magnification bias is defined as:

$$B(m) \equiv \frac{1}{N_{\rm Q}(m)} \int_{\Delta_{\rm min}}^{\infty} N_{\rm Q}(m+\Delta) p(\Delta) d\Delta$$
 (22)

where

$$N_{\rm Q}(m) \propto \begin{cases} 10^{a(m-m_{\rm o})}, & \text{if } m \le m_{\rm o} \\ 10^{b(m-m_{\rm o})}, & \text{if } m \ge m_{\rm o} \end{cases}$$
 (23)

(Note the quantity b above should not be confused with the quantity used earlier to describe the impact parameter for lensing.) We then calculate the magnification bias:

$$B(m) = \begin{cases} 0.8A_{\rm M}^2 \left[\left(\frac{1}{a - 0.8} + \frac{1}{0.8 - b} \right) 10^{(a - 0.8)(m_{\rm o} - m)} - \frac{1}{a - 0.8} A_{\rm M}^{(2.5a - 2)} \right] & \text{if } m \le m_{\rm o} - \Delta_{\min} \\ \frac{0.8}{0.8 - b} A_{\rm M}^{2.5b} 10^{(b - a)(m - m_{\rm o})} & \text{if } m_{\rm o} - \Delta_{\min} \le m \le m_{\rm o} \\ \frac{0.8}{0.8 - b} A_{\rm M}^{2.5b} & \text{if } m_{\rm o} \le m \end{cases}$$

$$(24)$$

Interestingly, b has to be less than 0.8 from the above formula in order to have a reasonable B(m). The observational value of b is well below 0.8 and will be presented later.

Next, as discussed in Fukugita & Turner [6], we have to average B(m) over the observed magnitude (m) distribution in order to obtain the relevant collective bias B(< m). We approximate a magnitude limited quasar survey using the selection function:

$$S(m) = \begin{cases} 1, & \text{when } m \text{ is less (brighter) than the survey limit} \\ 0, & \text{when } m \text{ is larger (dimmer) than the survey limit} \end{cases}$$
 (25)

and define

$$B(< m) \equiv \frac{\int_{m_{\min}}^{m} dm \int_{\Delta_{\min}}^{\infty} d\Delta p(\Delta) N_{Q}(m + \Delta)}{\int_{m_{\min}}^{m} dm N_{Q}(m)}$$
(26)

Using equation (23), we find

$$B(< m) = \frac{a(a-b)}{(a-0.8)(0.8-b)} \left(\frac{10^{0.8(m-m_o)} - 10^{0.8(m_{\min}-m_o)}}{10^{a(m-m_o)} - 10^{a(m_{\min}-m_o)}} \right) A_{\rm M}^2 - \frac{0.8}{a-0.8} A_{\rm M}^{2.5a}$$
when $m_{\min} \le m \le m_o - \Delta_{\min} < m_o$

$$B(< m) = \frac{1}{10^{a(m-m_{\rm o})} - 10^{a(m_{\rm min}-m_{\rm o})}} \left(\frac{b-a}{b} + \frac{0.8}{a-0.8} 10^{a(m_{\rm min}-m_{\rm o})} A_{\rm M}^{2.5a} + \frac{0.8a}{b(0.8-b)} 10^{b(m-m_{\rm o})} A_{\rm M}^{2.5b} - \frac{a(a-b)}{(a-0.8)(0.8-b)} 10^{0.8(m_{\rm min}-m_{\rm o})} A_{\rm M}^{2}\right)$$
when $m_{\rm min} \le m_{\rm o} - \Delta_{\rm min} \le m \le m_{\rm o}$

$$B(< m) = \frac{0.8a}{(0.8 - b)b} \left(\frac{10^{b(m - m_{\rm o})} - 10^{b(m_{\rm min} - m_{\rm o})}}{10^{a(m - m_{\rm o})} - 10^{a(m_{\rm min} - m_{\rm o})}} \right) A_{\rm M}^{2.5b}$$
when $m_{\rm o} - \Delta_{\rm min} \le m_{\rm min} \le m \le m_{\rm o}$

$$B(< m) = \left(\frac{0.8}{0.8 - b}\right) \frac{10^{b(m - m_{\rm o})} - 10^{b(m_{\rm min} - m_{\rm o})}}{\frac{b}{a} \left(1 - 10^{a(m_{\rm min} - m_{\rm o})}\right) + 10^{b(m - m_{\rm o})} - 1} A_{\rm M}^{2.5b}$$
when $m_{\rm o} - \Delta_{\rm min} \le m_{\rm min} \le m_{\rm o} \le m$

$$B(< m) = \frac{1}{b(1 - 10^{a(m_{\min} - m_o)}) + a(10^{b(m - m_o)} - 1)} \left(b - a + \frac{0.8b}{a - 0.8} 10^{a(m_{\min} - m_o)} A_{\rm M}^{2.5a} + \frac{0.8a}{0.8 - b} 10^{b(m - m_o)} A_{\rm M}^{2.5b} - \frac{ab(a - b)}{(a - 0.8)(0.8 - b)} 10^{0.8(m_{\min} - m_o)} A_{\rm M}^{2}\right)$$
when $m_{\min} \le m_o - \Delta_{\min} < m_o \le m$ (27)

2.3 Lensing statistics

We utilize a maximum likelihood method based on Poisson statistics in our analysis [20]. If we have a complete and flux limited quasar survey, then we can calculate the expected number of lensing events, N_{exp} , by summing up the probability of each quasar over all quasar samples, N_{Q} , i.e.,

$$N_{\rm exp} = \sum_{i=1}^{N_{\rm Q}} \tau(z_s = z_i)$$
 (28)

Using equations (7) and (28), we can write down the expected number density distribution, \mathcal{N}_i , which is the integrand of equation (7). If we choose small bin sizes for source redshift, galaxy redshift, and luminosity $\frac{L}{L^*}$, then there will be either no lensing events or one lensing event in each bin. Assuming appropriate Poisson probabilities $P_{0,i}$ and $P_{1,i}$, respectively, the likelihood function is

$$\mathcal{L} = \left[\prod_{i=1}^{N_{\text{obs}}} P_{1,i} \right] \left[\prod_{i=1}^{N_{\text{un}}} P_{0,i} \right]$$
(29)

where N_{obs} is the observed number of multiple-imaged lensing events, and N_{un} is the number of the un-lensed events. After taking the logarithm of \mathcal{L} , and taking the limit of summation to be an integral, we find the formula used in our lensing statistical analysis:

$$\ln \mathcal{L} = \sum_{l=1}^{N_{\text{obs}}} \ln \mathcal{N}_l - N_{\text{exp}} + \text{constant}$$
(30)

with

$$\ln \mathcal{N}_{l} \equiv \ln \frac{d^{2}\tau}{dz_{l} d\left(\frac{L}{L^{*}}\right)}$$

$$= \ln \left[\left(\frac{\sigma_{l}}{\sigma_{\rm DM}^{*}}\right)^{4} \left(\frac{y_{ol}y_{ls}}{y_{os}}\right)^{2} \frac{B(\langle m)f(\beta)}{\sqrt{\Omega_{o}(1+z_{l})^{3} + \Omega_{R}(1+z_{l})^{2} + \Omega_{\Lambda}}} \left(\frac{L_{l}}{L^{*}}\right)^{\alpha} \right] - \left(\frac{L_{l}}{L^{*}}\right) + \text{constant}$$
(31)

3 Velocity dispersions and luminosity functions: dark matter and galaxies

The probability of gravitational lensing can be seen, from equation (7) to depend strongly on both the luminosity function, and the velocity dispersion of galaxies. There is an explicit dependence on the latter in the lensing cross section. An implicit dependence arises as a result of the need to relate velocity dispersion to luminosity when performing the integral in equation (7). We have recently [21] explored the model dependent considerations associated with extracting the relevant velocity dispersions of galaxies from the data, in the context of finite core isothermal models. We review the chief results here, along with discussing the interdependence of these estimates on the assumed luminosity distribution of galaxies.

Returning to equation (1), we should bear in mind that the velocity dispersion in this equation, which is assumed to be independent of radius, cannot be measured directly. What we can measure is the line-of-sight velocity dispersion $\sigma_{los}(R)$, with the projected distance R

measured from the center of the observed galaxy (i.e., R is perpendicular to the line-of-sight to us). For a singular isothermal sphere, $\sigma_{\rm DM}$ is not a function of R, but $\sigma_{\rm los}\left(R\right)$ is, and this relationship is different when a galaxy has a finite core. Thus, one has to be careful how to use the measured velocity dispersion to derive the relevant quantity to utilize for lensing, namely whether it well approximates $\sigma_{\rm DM}$. Using a wide range of values of galaxy models, and self consistently solving the dynamical equations we demonstrated [21] that $\sigma_{\rm los}^2/\sigma_{\rm DM}^2$ is strongly sensitive to the core radius and galaxy anisotropy when the projected radius is less than $0.1R_{\rm e}$. This is consistent with observational data [22]. It can thus be dangerous to simply consider the line-of-sight velocity dispersion within $0.1R_{\rm e}$ as $\sigma_{\rm DM}$, even when core radii are small, as observations suggest they are for elliptical galaxies. However our results also indicated the following inequalities:

$$1.16 \le \frac{\sigma_{\rm DM}}{\sigma_{\rm los}(R)} \le 1.27$$
 at $R = 0.4R_{\rm e}$
 $1.20 \le \frac{\sigma_{\rm DM}}{\sigma_{\rm los}(R)} \le 1.30$ at $R = 0.54R_{\rm e}$
 $1.24 \le \frac{\sigma_{\rm DM}}{\sigma_{\rm los}(R)} \le 1.37$ at $R = R_{\rm e}$

These indicate that the intrinsic scatter of $\sigma_{\rm DM}$ will be less than 10 per cent if we can measure the line-of-sight velocity dispersion at $R_{\rm e}$ or half $R_{\rm e}$. Then, we can multiply this velocity dispersion by the average value (e.g. 1.25 for $R=0.54R_{\rm e}$), in order to get $\sigma_{\rm DM}$. This argument is almost independent of the core radius of each galaxy and the anisotropy parameter β .

More important, we demonstrated that measuring the central velocity dispersion of a galaxy can give a misleading representation of $\sigma_{\rm DM}$, and in particular can give an overestimate of $\sigma_{\rm DM}$ which can lead to a higher probability for lensing, and hence an inappropriately stringent bound on the cosmological constant.

Finally, the above estimates are for the case of a purely finite isothermal distribution. If one adds to this distribution some central mass, such as a large central black hole, this will further increase the central velocity dispersion, and also change the relationship between $\sigma_{\rm DM}$ and the line-of-sight velocity dispersion at $R_{\rm e}$ and half $R_{\rm e}$. By measuring the velocity dispersion at both these points, however, one can hope to extract out the central mass contribution and also the isothermal contribution [21]. (Alternately, it is clear that the velocity dispersion at $R_{\rm e}$ will be less sensitive to the former contribution, and thus can be used to approximate the isothermal contribution.) The important point here is that the mean impact parameter for lensing at redshifts greater than unity is of order 1-10 kpc. At this range a central mass, if it is of the order of $\approx 10^9 M_{\odot}$, contributes for example at the 5-10 percent level to the squared velocity dispersion, but it contributes merely at the 2-5 percent level to the bend angle for lensing by the galaxy at this distance (the bend angle at some radius r is $(2/\pi)$ times smaller for a point mass which has the same mass as an isothermal sphere at this radius, and hence produces the same velocity dispersion at this radius, because in the latter case the mass outside this radius contributes to the bend angle but not the velocity dispersion.) Since the fourth power of the velocity dispersion enters into the optical depth, interpreting a 10 per cent increase in the squared velocity dispersion using an isothermal sphere model predicts a 20 per cent increase in the optical depth, whereas the actual increase, if the contribution is from a central compact mass, is less than 10 per cent. Hence one must be concerned, when using velocity dispersions to estimate optical depths, about to what extent a possible central mass contributes to the former but not the latter.

To summarize these arguments one more time: The measured central velocity dispersion is not necessarily directly correlated to the quantity which is relevant for lensing statistics. This fact must be taken into account when attempting to utilize such statistics to constrain cosmological parameters.

The last step in the determination of $\sigma_{\rm DM}^*$ is the determination of the value of L^* and the relation between L and $\sigma_{\rm DM}$. We consider the former first. First, to be consistent, it is important to calculate the luminosity function in the same band as one estimates velocity dispersions, and in which one performs lensing searches. Second, it is important to consider not the luminosity function for all galaxies, but rather for E/S0 galaxies, as these dominate in the lensing statistics. An analysis of the latter has been carried out by Loveday et al. [16], and yields, in the B_J band the relation, for the Schechter function:

$$\alpha = 0.20; M^* = -19.71 + 5\log_{10} h$$
 (32)

In order to attempt to confirm this relationship in the $B_T(0)$ band we calculated [21] a luminosity function utilizing data from a subset of sample in Faber et al. [23] and de Vaucouleurs et al. [24]. In this case, we find a similar relation

$$\alpha = 0.15 \pm 0.55; M_{B_T(0)}^* = -19.66 + 5 \log_{10} h \pm 0.30$$
 (33)

Note that this best fit M^* differs from that used by Kochanek [9]. At the same time we stress a fact emphasized by Kochanek, there is a complicated interplay in the determination of both M^* and σ_{DM}^* , so that one cannot arbitrarily vary one without the other. In any case, we utilize our relation above for the $B_T(0)$ luminosity function in what follows below, although we also consider how our results would change if the parameters of the luminosity function change.

In order to estimate the velocity dispersion of L^* galaxies we found 42 galaxies with available velocity dispersions, 38 of which were appropriate for use in our analysis at $R = R_{\rm e}$, and 39 of which had reliable velocity measures at $R = 0.54R_{\rm e}$ [21]. When several different authors differed in their estimates of either $R_{\rm e}$ or $\sigma_{R_{\rm e}}$ we utilized the weighted mean of the different estimates and incorporated the scatter in our error estimate. We then calculated the least-square-fit of the relation between $\log_{10} (L/L^*)$ and $\log_{10} (\sigma_{R_{\rm e}}/{\rm km~s^{-1}})$ [21] and obtained

$$\log_{10}(L/L^*) = (-4.04 \pm 0.49) + (1.89 \pm 0.22)\log_{10}(\sigma_{R_e}/\text{km s}^{-1})$$
(34)

If we set $L = L^*$ in equation (34), then we find the velocity dispersion of luminous elliptical galaxies at the effective radius, $\sigma_{R_e}^* = 135.9 \pm 15 \text{ km s}^{-1}$. From the discussion above, we then multiply this number by 1.31, to get $\sigma_{\text{DM}}^* \approx 1.31 \sigma_{R_e}^* \approx 178 \text{ km s}^{-1}$.

Several issues are relevant to this result. In the first place, note that the L vs σ relation in the above equation differs from the standard Faber-Jackson relation [25]. Note however that this FJ relation is appropriate for central velocity dispersions. In addition, it may be there case that the elliptical galaxies do not form a uniform population, but rather that bright galaxies and faint galaxies follow separate Faber-Jackson curves (this point was raised to us by J. Peebles, who has been investigating this issue [26]). It thus may not be appropriate to enforce this relation on the bulk sample. To explore this latter possibility, and because it is galaxies with the largest velocity dispersions which will dominate in the analysis of lensing

statistics, we considered a subset of our galaxy sample with $\log_{10}(\sigma_{R_e}/\text{km s}^{-1}) > 2.2$ and rederived the L- σ relation. In this case, we found:

$$\log_{10}(L/L^*) = (-6.20 \pm 1.82) + (2.83 \pm 0.79) \log_{10}(\sigma_{R_e}/\text{km s}^{-1})$$
(35)

In this case, we find a somewhat higher value of $\sigma_{\rm DM}^*=203~{\rm km~s^{-1}}$ as might be expected given the features of this subsample. It is worth noting that we have used the technique described earlier of using line-of-sight velocity dispersions at two values of R to extract out the asymptotic velocity dispersion which may be most appropriate for lensing, and find, coincidentally that for this subsample a value $\sigma_{\rm DM}^*=179~{\rm km~s^{-1}}$. Nevertheless, as a probe of the robustness of the gravitational lensing constraints we incorporate both of the above relations as well as the direct inferred values of $\sigma_{\rm DM}^*$ in our analysis. Note also that increasing the slope in the L vs $\sigma_{\rm DM}$ relation has the same effect on lensing as decreasing α in the Schechter function, thus once again demonstrating the interdependence of these quantities in the deriving constraints.

Finally, having derived two estimates for $\sigma_{\rm DM}^*$ here, we must note that the lower value $\sigma_{\rm DM}^* \approx 178~{\rm km~s^{-1}}$ is smaller than that utilized in several previous lensing statistical analyses. This may be due in part to what we claim is the inappropriate use of central velocity dispersions in other analyses, and while we reiterate that the value of $\sigma_{\rm DM}^*$ cannot be independently varied in a self consistent analysis, and depends upon the form of the luminosity function, in order to allow for large possible systematic errors, we also used $\sigma_{\rm DM}^* \approx 207~{\rm km~s^{-1}}$, which corresponds to a 2σ variation in the fit to $\sigma_{\rm DM}^*$ from first relation (42) above. Last, for purposes of comparison with Kochanek [9], we considered an even larger $\sigma_{\rm DM}^*$ value, while at the same time adopting his choice of values for the Schechter function $\alpha = -1$, L vs σ slope of 4, (and setting $r_{\rm c} = 0$ in this case, see below) in order to explore the effects of variation in choice of M^* and sample selection.

4 Review of core radius

The final quantity which we must determine in order to carry out our analysis is the relationship between the core radius of E/S0 galaxy and its luminosity. In Table 3, we list the inferred values of core radii from the Class I data in Lauer [?], distances of galaxies from Faber et al. [23], and apparent magnitudes (B_T(0)) from de Vaucouleurs et al. [24]. With $M_{B_T(0)}^* = -19.66 + 5 \cdot \log_{10} h \pm 0.30$, $\log_{10}(\frac{L}{L^*})$ for each galaxy in Table 3 can be calculated. We plot $\log_{10}(\frac{L}{L^*})$ against $\log_{10}(r_c/(h^{-1}p_c))$ in Figure 2. With 13 samples in Table 3, we have found the best fit is $\frac{r_c}{r_c^*} = (\frac{L}{L^*})^{1.65}$ with $r_c^* = 45 \, h^{-1}p_c$ and $\chi^2 = 11$. If we consider $\Delta \chi^2$ at the 95 per cent confidence level with three parameters of interest (i.e., r_c^* , L^* , and a power law relation between r_c and L), such that the total $\chi^2 = 18.8$ (which is the 95 per cent confidence contour line), with the power law relation and L^* fixed, then we have $r_c^* = 45 \, ^{+25}_{-17} h^{-1}p_c$. The best fit value of r_c^* would in fact agree with an earlier investigation, if we neglect uncertainties from distances of galaxy samples, and normalize $M_{B_T(0)}^*$ to the value chosen in Krauss & White [7].

An interesting test of this fit is to estimate the r_c of NGC 7457, which is an S0 galaxy in Lauer et al. [27]. Its apparent magnitude ($B_T(0)$) is 11.76 from de Vaucouleurs et

al. [24], and its distance is about $10 \ h^{-1}{\rm Mpc}$. Based on the formula in this section, we obtain $r_{\rm c} = 5.2 \ h^{-1}{\rm pc}$ for the best fit of $r_{\rm c}^*$, and the 95 per cent confidence lower limit is $r_{\rm c} = 3.2 \ h^{-1}{\rm pc}$. This result is marginally consistent with the lack of evidence for a core radius of NGC 7457 at a limit of $\approx 3.4 \ {\rm pc}$ (H_o = 80 km s⁻¹ Mpc⁻¹) [27].

In our analysis, with the parameters given above and later, without including magnification bias, we have found that the lensing probability is reduced due to the core radius by a factor 2 to 3, depending on the value of $\Omega_{\rm o}$ in flat cosmological models. With the magnification bias included, this reduction factor will be significantly decreased [9]. However, one important result of our analysis is that these effects need not cancel out completely, depending upon parameters of the luminosity function, so that as we shall see, the introduction of a finite core can in fact suppress the optical depth for lensing, even when magnification bias is taken into account.

5 Quasar samples and lensing events

5.1 Quasar samples

We first utilized the Large Bright Quasar Survey (LBQS) catalogue of Hewett, Foltz & Chaffe [28]. There are 1055 quasar samples in that catalogue. All quasars are between redshift 0.2 and 3.4, and their apparent magnitudes (B_J) are between 16 and 18.9. We include these flux limits to calculate the magnification bias in our statistics. There was only one lensing event, LBQS1009-0252, observed in this survey.

As a comparison, we also used the Snapshot survey by Maoz et al. [29] combined with other surveys by Crampton, McClure & Fletcher [30], Surdej et al. [31], and Yee, Filippenko & Tang [32]. There are 648 quasars in this total sample set. There were 4 lensing events in these surveys. In modelling the magnification bias for this set we utilized the flux limit of 19.5, appropriate for the Snapshot survey, which contains the largest number of quasars, slightly more than the Surdej et al. survey. Our results do not depend sensitively on this choice, however, and in any case the flux limit in the latter survey is similar to that in the Snapshot survey.

Finally, if we consider all five surveys together, then we will have 1615 quasars in total, with five lensing events. In our analysis of this combined sample we again utilized the flux limit from the Snapshot survey (lower than that for the LBQS survey) to calculate the magnification bias.

5.2 Lensing events

Kochanek [8, 9] has previously discussed the rationale for considering the 5 strong gravitational lensing events mentioned above among all optical gravitational lensing candidates for use in the calculation of lensing statistics. We list the quasar redshifts, lens redshifts, and angular splittings for these events in Table 4 [33, 34, 35, 36, 37, 38, 39]. In order to apply our statistical model, we actually need to know the redshift of each lens. At present, only the redshifts of lenses in two systems (Q0142-100 and PG1115+080) have been firmly measured. For those lenses which lack galaxy redshift information, we chose the most likely

absorption lines as lens redshifts. For systems H1413+117 and Q1208+1011, we used two possible redshifts in our analysis, as two different lenses are possible candidates.

With the information in Table 4, we can calculate the likelihood function in equation (32). What we need are the core radius and velocity dispersion for each galaxy. Recall the angular separation is well approximated by $\Delta\theta = 2\sqrt{1-2\beta} \alpha_0 \frac{y_{ls}}{y_{os}}$ [19]. Using the results of section 3, we employ power law relations between luminosity and velocity dispersion as either $\frac{L}{L^*}$ $(\frac{\sigma_{\rm DM}}{\sigma_{\rm DM}^*})^{\gamma}$, with (1) $\gamma=1.89, \sigma_{\rm DM}^*=178$ km, s⁻¹ or (2) $\gamma=2.83, \sigma_{\rm DM}^*=203$ km s⁻¹. This implies a power law relation between core radius and velocity dispersion, i.e., $\frac{r_{\rm c}}{r_{\rm c}^*}=(\frac{\sigma_{\rm DM}}{\sigma_{\rm DM}^*})^{3.12}$ or $\frac{r_c}{r_c^*} = \left(\frac{\sigma_{\rm DM}}{\sigma_{\rm DM}^*}\right)^{4.67}$. Combining this equation with a known $\Delta\theta$ value, and with a given cosmological model, in principle, we can solve r_c and $\sigma_{\rm DM}$ for each lensing galaxy. Actually, except for the lensing galaxy for the system Q1208+1011, all other four lensing systems allow a second solution with $\sigma_{\rm DM}$ at least 1400 km s⁻¹, which is not a suitable scale for a galaxy. In our analysis we select the smaller but reasonable velocity dispersion. In Tables 5 and 6, we list our theoretical predictions of $\sigma_{\rm DM}$, $r_{\rm c}$, and $B_{\rm T}(0)$ for the lensing galaxy for each lensing system in different cosmological models. Note that the inferred $\sigma_{\rm DM}$ values are reasonable, but have an average which exceeds the value of $\sigma_{\rm DM}^*$ we have used. This is to be expected. Lensing galaxies will have preferentially larger velocity dispersions than the mean, simply because these galaxies are weighted more heavily in the probability function. It would thus be inappropriate to use the mean for lensing galaxies to model all galaxies.

For the five events considered here, we find that that $\frac{\sigma_{\rm DM}}{\sigma_{\rm DM}^*}$ (or $\frac{L}{L^*}$) increases when $\Omega_{\rm o}$ increases for all five events in flat universe models. This can be explained as follows: $y_{os}/(y_{ol}y_{ls})$ increases when $\Omega_{\rm o}$ increases for a fixed source redshift and a fixed lens redshift [7, 40]. For a fixed (observed) $\Delta\theta$, when $y_{os}/(y_{ol}y_{ls})$ increases, $\frac{\sigma_{\rm DM}}{\sigma_{\rm DM}^*}$ has to increase in order to prevent β from approaching 1/2. The $\frac{\sigma_{\rm DM}}{\sigma_{\rm DM}^*}$ ratio as a function of $\Omega_{\rm o}$ seems to increase faster when $\Delta\theta$ is smaller. In fact, there is no solution for $r_{\rm c}$ and $\sigma_{\rm DM}$ of the system Q1208+1011 when $\Omega_{\rm o} \geq 0.95$, if $z_l = 2.9157$ is chosen. This is because $\frac{y_{ls}}{y_{os}}$ decreases when $\Omega_{\rm o}$ increases for a fixed source redshift and a fixed lens redshift. As a result, $\Delta\theta$ from the system Q1208+1011 is too 'large' in the $\Omega_{\rm o} = 1$ universe model if the given source redshift and lens redshift are accurate and correct. If more 'large' angular splitting lensing systems are observed at high redshifts, this will more strongly favor a low matter density universe, although of course the number of lensing events will play an important role in constraining models. In open universe models, the results are similar to flat universe models, but the $\frac{\sigma_{\rm DM}}{\sigma_{\rm DM}^*}$ ratio as a function of $\Omega_{\rm o}$ is smoother.

6 Numerical results

6.1 Magnification bias

With the parameters discussed above, we can calculate the lensing optical depth. One interesting task is to compare our bias factor to the SIS model in Fukugita & Turner [6]. We define the average of B(< m) as following:

$$\langle B(\langle m)\rangle \equiv \frac{1}{\tau} \int B(\langle m)d\tau \tag{36}$$

where τ is the optical depth of the lensing events. In addition to the parameters discussed previously, We choose m_{\min} to be 16, $m_o = 19.15$, a = 0.86, b = 0.28 from Hartwick & Schade [41]. In Figure 3, we have plotted $\langle B(\langle m)\rangle\rangle$ as a function of quasar (source) redshift in different cosmological models, with m = 18.9, 19.5, and 22.

Although we set a lower limit for the integrals in equation (26), there is no significant impact if we choose m_{\min} to be either 16 or smaller (such as negative infinity as in Fukugita & Turner [6]). In Figure 3, we have shown that $\langle B(< m) \rangle$ is almost a constant at higher source redshift $(z_s \geq 1)$ in each cosmological model. Although the optical depth of the $\Omega_{\Lambda} = 1$ flat universe model is larger than the optical depth of the $\Omega_{\rm o} = 1$ universe model, the averaged total magnification bias goes in the other direction. This is also true in the open universe model. Comparing to the bias values in Fukugita & Turner [6], we have $\langle B(< m) \rangle$ around 13 when m = 18.9, but they have 7.33. We have $\langle B(< m) \rangle$ around 7, but they have $\langle B(< m) \rangle = 4.25$, when $\langle B(< m) \rangle = 4.25$,

6.2 Flat universe models

Incorporating the magnification bias results discussed above we first consider the statistical analysis in which quasars from all 5 surveys were utilized. For flat universe models, these are presented in columns 2 to 7 in Table 7. As mentioned earlier, the apparent magnitude of the combined quasar survey limit has been set to be 19.5. If we consider our best fit galaxy parameters it is clear from columns 2 to 5 that the expected number of lenses is a good fit, and the likelihood function is minimized, when $\Omega_o \approx 0.2$. The strict 95 per cent confidence level (for 1 degree of freedom) on this quantity for these galaxy parameters ranges from $0.07 < \Omega_{\rm o} < 0.55$ (column 3) or $0.07 < \Omega_{\rm o} < 0.65$ (column 5). However, if we consider the intrinsic scatter merely in velocity dispersions and core radii, then we find a different result. For example, consider a smaller r_c^* , 28 h^{-1} pc, and a larger σ^* , 207 km s⁻¹. Columns 6 and 7 show a best fit around $\Omega_{\rm o}=0.5$, and the 95 per cent confidence level is $\Omega_{\rm o}>0.24$. This result here is comparable, although less stringent than the result (with $\Omega_0 = 1$ as the best fit value) given in Kochanek [9], without including core radii effects. This demonstrates the sensitivity of existing statistical constraints to the values of the assumed velocity dispersions and core radii. Note that the inclusion of core radii, and the difference in the assumed value of M^* presumably account for the reduction in the minimum allowed value of $\Omega_{\rm o}$ compared to Kochanek [9]. Also note that inclusion of core radii is largely responsible for shifting the peak of the likelihood function in this case toward values lower than $\Omega_0 = 1$. In any case, while suggesting that $\Omega_0 < 1$ is preferred by our best fit parameters, the divergence in results demonstrates the sensitivity of existing statistical constraints to the values of the assumed velocity dispersions and core radii. The likelihood functions mentioned above are plotted in Figure 4.

Setting $\Omega_{\rm o} = 0.2$ in Figure 5, we plot the expected number of lensing events and the

observed (five) events vs source redshift (z_s) . The shape of the predicted curve is in agreement with the observation, given the very limited statistics. If one had a complete quasar survey up to a high redshift (larger than 2.5), one could use this shape function to probe more clearly the agreement, or lack thereof, between theory and observation.

In columns 8 to 13 in Table 7, we list results obtained by using only the LBQS survey and the single lens candidate, LBQS1009-0252. Because only one lens is considered, the results more strongly favor a higher $\Omega_{\rm o}$ universe. Nevertheless, while the best fit of $\Omega_{\rm o}$ is around 0.8, the 95 per cent confidence level lower limit is about $\Omega_{\rm o} > 0.15$. The large width of the allowed region presumably reflects both the reduced statistics, and the effect of non-zero core radii. The likelihood functions are plotted in Figure 6. Columns 12 and 13 involve the parameters used in Kochanek [9] (i.e., $\alpha = -1$, $\gamma = 4$, $r_{\rm c}^* = 0$, $\sigma^* = 225$ km s⁻¹). The best fit of $\Omega_{\rm o}$ from the likelihood analysis is 0.95, with 95 per cent confidence level, $\Omega_{\rm o} > 0.2$ in flat universe models (see also Figure 6). This result is consistent with the result given by Kochanek [9], but again the lower limit on $\Omega_{\rm o}$ is reduced.

For comparison, in columns 14 to 16 the result using the four combined quasar surveys [29, 30, 31, 32] without LBQS are shown. As expected this tends to favor slightly smaller $\Omega_{\rm o}$ than the five survey analysis. The best fit of $\Omega_{\rm o}$ is about 0.15. The 95 per cent confidence levels are $0.03 < \Omega_{\rm o} < 0.43$ and $0.03 < \Omega_{\rm o} < 0.38$ for the last two columns. Statistical values are not available at high $\Omega_{\rm o}$ values in the last two columns, because $\sigma_{\rm DM}$ and $r_{\rm c}$ of the lensing galaxy in system Q1208+1011 cannot be fitted, as discussed in the previous section.

As another probe of the galaxy lensing parameters, if we define the mean angular splitting as

$$<\Delta\theta> \equiv \frac{1}{\tau} \int \Delta\theta d\tau$$
 (37)

with $\Delta\theta=2\sqrt{1-2\beta}~\alpha_0\frac{y_{ls}}{y_{os}}$ [19], we find that $<\Delta\theta>\approx 2''.9~(\gamma=1.89,\sigma_{\rm DM}^*=178~{\rm km~s^{-1}})$ or $2''.0~(\gamma=2.83,\sigma_{\rm DM}^*=203~{\rm km~s^{-1}})$, when the source redshift is less than 5 in flat universe models. However, if we calculate the mean value of the angular separation from Table 4, we find a mean value 1''.542. From the formula of $<\Delta\theta>$ for the SIS model [8], one can reduce the mean angular splitting by either decreasing σ^* or increasing the value of the parameter γ (for fixed Schechter α). Indeed, if we choose $\sigma_{\rm DM}^*=178~{\rm km~s^{-1}}$ and $\gamma=2.83$, the combination suggested by extracting away the central mass contribution from the asymptotic velocity dispersion as discussed previously, we find $<\Delta\theta>\approx 1''.5$. From Figure 4, one can infer in this case a best fit for $\Omega_{\rm o}$ around 0.23, with a 95 per cent confidence interval around $0.07 < \Omega_{\rm o} < 0.6$.

6.3 Open universe models

We repeat the above analysis for open universe models. When all 5 surveys are included in the analysis the results are displayed in columns 2 to 5 in Table 8. In this case the best fit is $\Omega_{\rm o}\approx 0$. Note, that the expected number of lensing events is smaller than the observed number when one considers more realistic values $\Omega_{\rm o}>0$ in this case. The 95 per cent confidence limits are nevertheless fairly broad, with either $\Omega_{\rm o}<0.65$ (column 3) or $\Omega_{\rm o}\leq 1$ (column 5).

We next consider just the four quasar surveys (Crampton et al. [30], Maoz et al. [29], Surdej et al. [31], and Yee et al. [32]). The results are listed in columns 6, 7, and 8 in

Table 8. The best fit value is again $\Omega_o = 0$, with a 95 percent confidence limit of $\Omega_o < 0.3$ in this case.

Finally, if we consider the LBQS survey alone, with a single lensed event, it is clear that higher density open universe models will fare better. Since in fact the best fit value of $\Omega_{\rm o}$ is in this case close to 0.95, the open universe model likelihood function in this region is then very similar to that for the flat model. As a result, the likelihood function and predicted number of events will have the same behavior (near $\Omega_{\rm o}=1$) as the values shown in columns 8-13 of Table 7 and displayed in Figure 6 for the flat universe case. As a result, we do not explicitly re-display the values again in Table 8.

In general open universe models tend to predict a redshift distribution for the lenses which is in poorer agreement with observation, although again because of the very limited statistics this is not a quantitative problem at this point. It is also worth noting that one can increase the number of lensing events by increasing $\sigma_{\rm DM}^*$ as seen in column 4, but in this case the mean predicted angular splitting will be increased, as we have discussed in the previous subsection.

7 Conclusions

The various different fits described here in Tables 7 and 8 demonstrate that the constraints one derives on cosmological models from existing lensing statistics depend in detail on the parameters one uses to model galaxy distributions. Nevertheless, the model parameters which we suggest are favored involve a low density, cosmological constant dominated universe—the model which coincidentally is favored by other astrophysical data at the present time. In our analysis, we have been careful to self consistently obtain the various lensing parameters (velocity dispersions, core radius, magnification bias, etc.). As a result, the general features of our analysis are expected to be robust, even though the intrinsic scatter in values of the selection functions, galaxy velocity dispersions and galaxy core radii may be large at the present time. Although the selection function in this paper is as simple as in Fukugita & Turner [6], a real selection function should at least account for the image separation and flux ratio. If we include these factors in our paper, they will reduce the number of predicted lensing events. With the observed number of lensing events remaining unchanged, this means that the lensing statistics will favor a flat universe with a larger cosmological constant value—in even greater disagreement with Kochanek's conclusion [9]. Quantitatively our analysis suggests a best fit value of Ω_0 ranges between 0.25-0.55 in a flat universe if five lensing events in the 5 optical surveys considered here are incorporated. (Note however that this value can raise to 0.95 if only one lensing event and a single survey are included in the analysis.) The distribution of predicted events is in a good agreement with the distribution of observed events in source redshift space (see Figure 5). Note however that the results depend on which lensing surveys are utilized and thus the number of lenses used. Clearly what is required in order to distinguish between model parameters are greater statistics from a complete full sky quasar survey up to high redshift.

The predicted number of lenses in open universe models do not vary as sharply as flat universe models do over the range of $\Omega_{\rm o}$, so while the preferred value of $\Omega_{\rm o}$ is around 0 if lensing events from all five lensing surveys considered here are incorporated, the allowed

range remains very broad. The fact that open universe models tend to predict too few events when compared to 5 lensing events in the five surveys has also been demonstrated by Chiba & Yoshii [13]. Note that even if a larger $\sigma_{\rm DM}^*$ is chosen compared to those utilized here, in order to increase the number of lenses, then the mean angular splitting will become larger than the mean value of the observations in this case. Finally, open universe models tend to predict more lower redshift lenses than flat universe models, and this may be a useful discriminant in the future.

We remind readers that the lensing optical depth is proportional to the fourth power of the velocity dispersion. A 10 per cent change of velocity dispersion can cause 46 per cent change in the optical depth. Thus, better estimates of velocity dispersions for E/S0 galaxies are necessary before the statistical limits can improve. We have argued here that determining the appropriate velocity dispersion for use in lensing statistics, when core radii are not zero can be somewhat subtle. Self consistent modelling of the gravitational potentials may be necessary before line-of-sight velocity dispersions can be used to infer dark matter velocity dispersions. In addition, the effect of compact central mass conglomerations may bias the interpretation on extracts from using central velocity dispersions in the derivation of lensing statistics.

The parameter γ , relating velocity dispersion and luminosity is also important in gravitational lensing studies. A larger value of γ reduces the mean angular splitting and also pushes $\Omega_{\rm o}$ toward a low value and a narrow 95 per cent confidence level. (These effects can be easily understood from equations (28) and (32).) Therefore, improved observations of E/S0 galaxy velocity dispersions along with luminosity measurements in order to reduce the intrinsic scatter in the data as well as to better model the Schechter parameters would be useful.

We have also demonstrated that adding a core radius in the lensing analysis will generally reduce the total optical depth, even though the magnification bias factor will be higher than that predicted SIS models. The overall reduction of the lensing optical depth for non zero core radii is parameter dependent, however. For example, if we choose a steeper power law relation between the velocity dispersion and the luminosity $(L \propto \sigma^4)$, with Schechter $\alpha = -1$, then including a core radius in the analysis produces no significant change in the number of expected lensing events, and produces shifts in the best fit likelihood analysis for Ω_0 of ≤ 0.1 . With a shallower power law relation and the Schechter parameters used in this paper, we have however found a 30 per cent to 40 per cent change of the number of predicted lensing events by adding a core radius. This result is easily understood: a shallow power law effectively more strongly weights larger core radii when L is less than L^* .

Although the apparent magnitudes are given in $B_T(0)$ band without K-corrections in Tables 5 and 6, these values nevertheless suggest why observers have not yet found the lensing galaxy in systems H1413+117, LBQS1009-0252, and Q1208+1011. We also suggest examining system Q1208+1011 carefully, because this event, because of its angular splitting and assumed the high lens redshift, helps drive the fits to a low Ω_o universe. Note that recent studies of the faint lens image of H1413+117 suggest a value of the lens brightness consistent with that calculated in Table 5 [42, 43].

To summarize: the self consistent incorporation of core radii in galaxy models, and fitting the distribution of galaxies to the E/S0 galaxies which dominate lensing statistics combine together to suggest a statistical best fit of predictions to the results of existing optical quasar

lensing surveys for a flat universe model with $\Omega_{\rm o}$ in the range 0.25-0.55. Considerable systematic uncertainty persists however in the appropriate velocity dispersion to use in models, as well as the luminosity-velocity dispersion relation, and the determination of the appropriate luminosity function parameters. In addition, how to appropriately combine the results of different surveys by different groups is not obvious. Since the results depend upon all these factors, it may be premature to argue definitively in favor of this best-fit scenario, although it is encouraging that it agrees with that obtained using other cosmological observables. In any case, we have derived here several new results here associated with magnification biasing and galaxy models with core radii, as well as the determination of the appropriate velocity dispersion to use in galaxy lensing models. As data improves, we expect that the techniques described here will be useful in further constraining theoretical models.

Acknowledgments

This research work has been partially supported by the Industrial Physics Group in the Physics Department at Case Western Reserve University, and by a grant from DOE. This research has also made use of the NASA/IPAC Extragalactic Database (NED) which is operated by the Jet Propulsion Laboratory, California Institute of Technology, under contract with the National Aeronautics and Space Administration. We thank Jim Peebles for discussions, and informing us of his work in progress.

References

- [1] L. M. Krauss and M. S. Turner, General Relativity Gravitation 27, 1137 (1995).
- [2] J. P. Ostriker and P. Steinhardt, Nat. 377, 600 (1995).
- [3] L. M. Krauss, Astrophys. J. **501**, 461 (1998).
- [4] S. Perlmutter et al., LBNL preprint 41801, 1998.
- [5] A. G. Riess et al., Astron. J. 116 1009 (1998).
- [6] M. Fukugita and E. L. Turner, Mon. Not. R. Astron. Soc. 253, 99 (1991) (FT).
- [7] L. M. Krauss and M. White, Astrophys. J. 394, 385 (1992).
- [8] C. S. Kochanek, Astrophys. J. 419, 12 (1993).
- [9] C. S. Kochanek, Astrophys. J. 466, 638 (1996).
- [10] C. S. Kochanek, Astrophys. J. 436, 56 (1994).
- [11] G. Hinshaw and L. M. Krauss, Astrophys. J. 320, 468 (1987) (HK).
- [12] E. L. Turner, J. P. Ostriker, and J. R. Gott, Astrophys. J. 284, 1 (1984) (TOG).
- [13] M. Chiba and Y. Yoshii, Astrophys. J. 489, 485 (1997).

- [14] M. Chiba and Y. Yoshii, Astrophys. J. **510**, 42 (1999).
- [15] M. Postman and M. J. Geller, Astrophys. J. 281, 95 (1984).
- [16] J. Loveday, B. A. Peterson, G. Efstathiou, and S. J. Maddox, Astrophys. J. 390, 338 (1992).
- [17] P. J. E. Peebles, *Principles of Physical Cosmology* (Princeton University Press, Princeton, 1993).
- [18] P. L. Schechter, Astrophys. J. **203**, 297 (1976).
- [19] Y.-C. N. Cheng and L. M. Krauss, Astrophys. J. **514**, 25 (1999).
- [20] T. J. Loredo and D. Q. Lamb, Ann. N.Y. Acad. Sci. 571, 601 (1989).
- [21] Y.-C. N. Cheng and L. M. Krauss, 1999, CWRU-P28-99.
- [22] R. Bender, R. P. Saglia, and O. E. Gerhard, Mon. Not. R. Astron. Soc. 269, 785 (1994) (BSG).
- [23] S. M. Faber, G. Wegner, D. Burstein, R. L. Davies, A. Dressler, D. Lynden-Bell, and R. J. Terlevich, *Astrophys. J. Suppl.* **69**, 763 (1989) (7s).
- [24] G. de Vaucouleurs, A. de Vaucouleurs, H. G. Jr. Corwin, R. J. Buta, G. Paturel, and P. Fouqué, *Third Reference Catalogue of Bright Galaxies* (Springer-Verlag, New York, 1991) (RC3).
- [25] S. M. Faber and R. E. Jackson, Astrophys. J. 204, 668 (1976).
- [26] P. J. E. Peebles and M. Fukugita, 1999, astro-ph/9906036.
- [27] T. R. Lauer et al., Astrophys. J. Lett. 369, L41 (1991).
- [28] P. C. Hewett, C. B. Foltz, and F. H. Chaffee, Astron. J. 109, 1498 (1995) (LBQS)
- [29] D. Maoz et al., Astrophys. J. 409, 28 (1993) (Snapshot).
- [30] D. Crampton, R. D. McClure, and J. M. Fletcher, Astrophys. J. 392, 23 (1992).
- [31] J. Surdej et al., Astron. J. 105, 2064 (1993).
- [32] H. K. C. Yee, A. V. Filippenko, and D. Tang, Astron. J. 105, 7 (1993).
- [33] J. Surdej et al., Nat. 329, 695 (1987) (Q0142-100).
- [34] P. Magain, J. Surdej, J.-P. Swings, U. Borgeest, R. Kayser, H. Kühr, S. Refsdal, and M. Remy, Nat. 334, 325 (1988) (H1413+117).
- [35] P. Magain, J. Surdej, C. Vanderriest, B. Pirenne, and D. Hutsemékers, Astron. and Astrophys. Lett. 253, L13 (1992) (Q1208+1011).

- [36] P. C. Hewett, M. J. Irwin, C. B. Foltz, M. E. Harding, R. T. Corrigan, R. L. Webster, and N. Dinshaw, Astron. J. 108, 1534 (1994) (Q1009-0252).
- [37] S. Refsdal and J. Surdej, Rep. Prog. Phys. **56**, 117 (1994) (PG1115+080).
- [38] P. Helbig and R. Kayser, Astron. and Astrophys. 308, 359 (1996) (PG1115+080).
- [39] A. Siemiginowska, J. Bechtold, T. L. Aldcroft, K. K. McLeod, and C. R. Keeton, Astrophys. J. 503 118 (1998) (Q1208+1011).
- [40] M. Fukugita, T. Futamase, M. Kasai, and E. L. Turner, Astrophys. J. 393, 3 (1992).
- [41] F. D. A. Hartwick and D. Schade, Ann. Rev. Astron. Astrophys. 28, 437 (1990).
- [42] D. A. Turnshek, O. L. Lupie, S. M. Rao, B. R. Espey, and C. J. Sirola, Astrophys. J. 485, 100 (1997).
- [43] J.-P. Kneib, D. Alloin, and R. Pelló, Astron. and Astrophys. Lett. 339, 65 (1998).

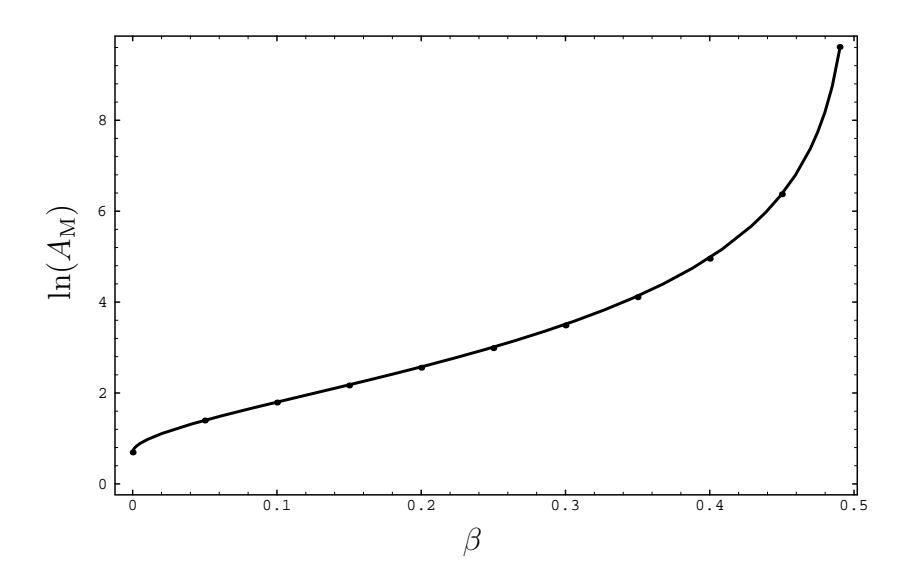


Figure 1: Plot of natural logarithm of $A_{\rm M}$ versus parameter β . The dots are numerical results, and the solid curve is the best fit curve: $2/(L_{\rm o}^{0.65})$.

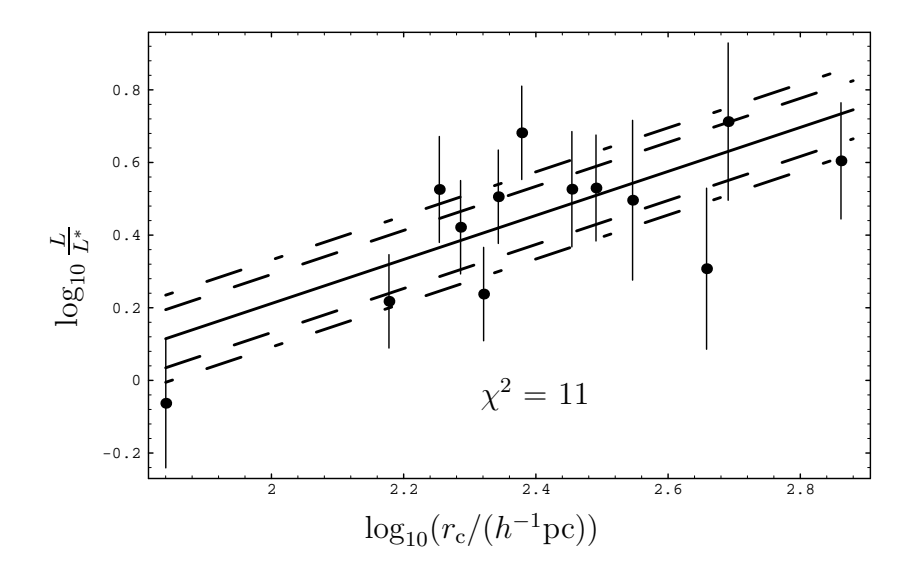


Figure 2: The best fit plot of $\log_{10}\frac{L}{L^*}$ vs $\log_{10}(r_{\rm c}/(h^{-1}{\rm pc}))$. There are 13 samples with error bars shown in the figure. The middle solid line is the best fit, and the two dash lines give the 68 per cent confidence level, assuming the best fit power law. The two dash-dot lines give the 95 per cent confidence level under the same condition.

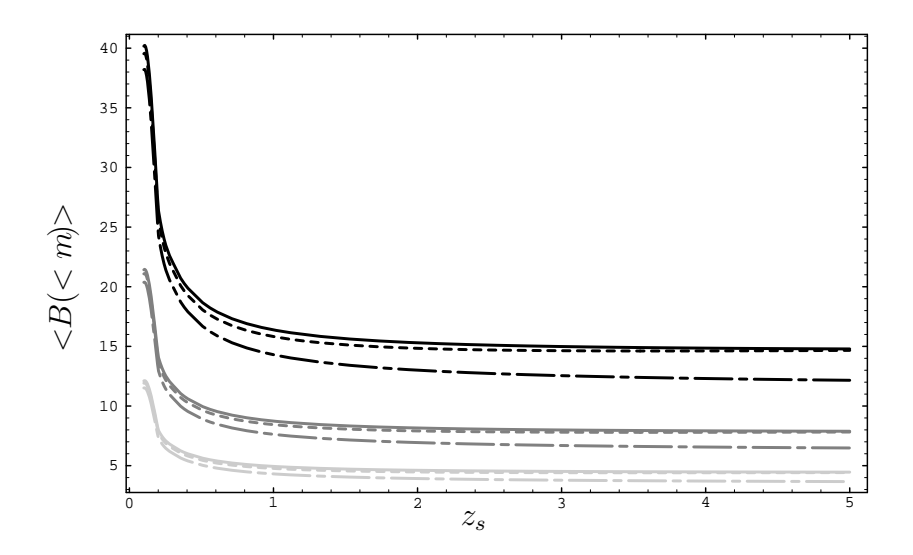


Figure 3: Plots of $\langle B(\langle m)\rangle$ versus quasar (source) redshift. The solid curve sets are for a flat universe model, with $\Omega_{\rm o}=1$. The dash-dot curve sets are also for a flat universe model, but with $\Omega_{\rm o}=0$, and $\Omega_{\Lambda}=1$. The dot-dot curve sets are for an open universe model, with $\Omega_{\rm o}=0$ and zero cosmological constant. The black (highest) curves represent quasar survey limit, m=18.9. The gray curves represent quasar survey limit, m=19.5. The light gray (lowest) curves represent quasar survey limit, m=22. We choose $\sigma_{\rm DM}^*=178~{\rm km~s^{-1}}$, $r_{\rm c}^*=45h^{-1}$ pc, and $\gamma=1.89$ to generate these curves.

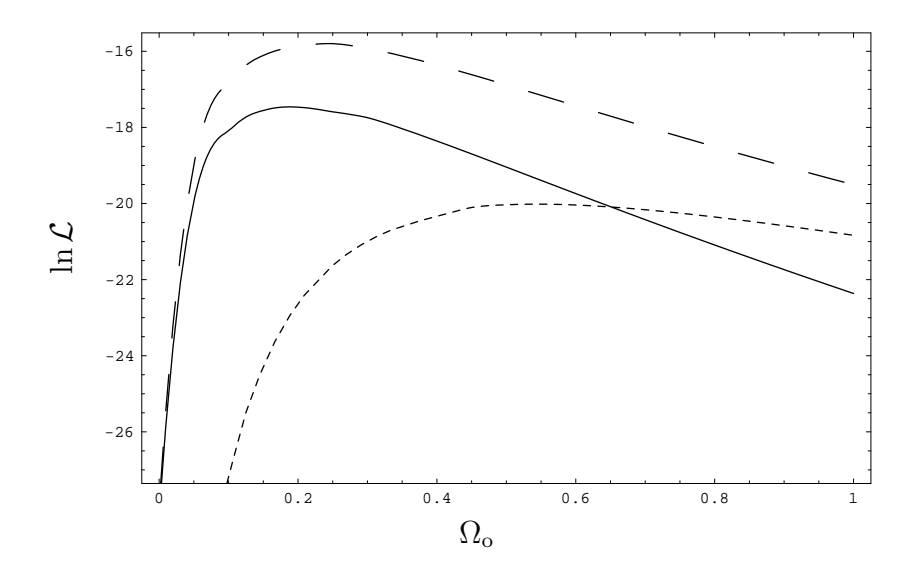


Figure 4: Plots of likelihood functions vs $\Omega_{\rm o}$. The solid curve is the plot of the third column in Table 7, with $r_{\rm c}^*=45~h^{-1}{\rm pc},~\sigma_{\rm DM}^*=203~{\rm km~s^{-1}},~{\rm and}~\gamma=2.83$. The dash-dash curve represents the result for $r_{\rm c}^*=45~h^{-1}{\rm pc},~\sigma_{\rm DM}^*=178~{\rm km~s^{-1}},~{\rm and}~\gamma=1.89$. The dot-dot curve is the plot for $r_{\rm c}^*=28~h^{-1}{\rm pc},~\sigma_{\rm DM}^*=207~{\rm km~s^{-1}},~{\rm and}~\gamma=1.89$.

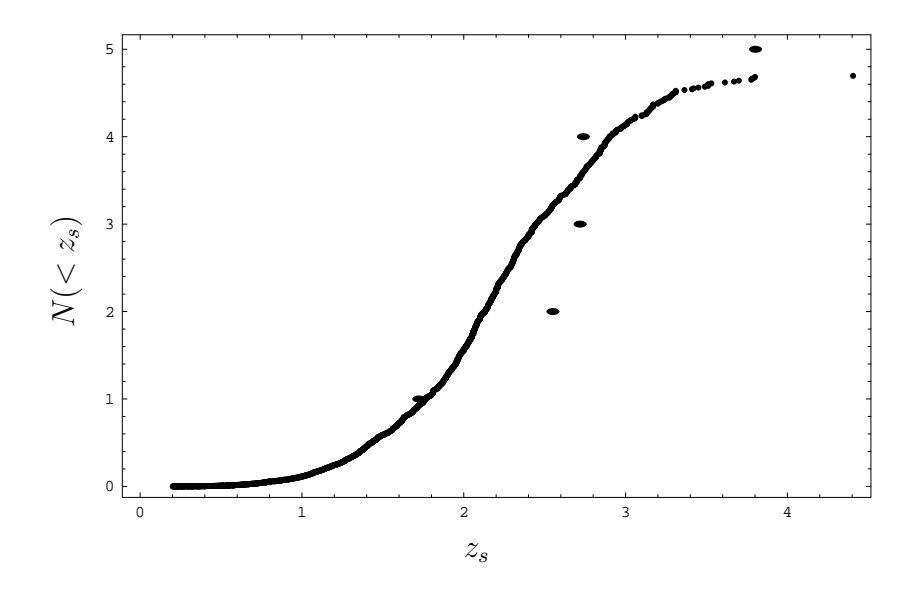


Figure 5: The predicted number of events and observed events are plotted as a function of quasar redshifts from all 5 quasar surveys with $\Omega_{\rm o}=0.2$ in a flat universe model. The small dots making up the curve give the total predicted number of lensing events within a given source redshift. The ellipses give the number of observed events. The parameters are $\sigma_{\rm DM}^*=203~{\rm km~s^{-1}},\,r_{\rm c}^*=45h^{-1}$ pc, and $\gamma=2.83$.

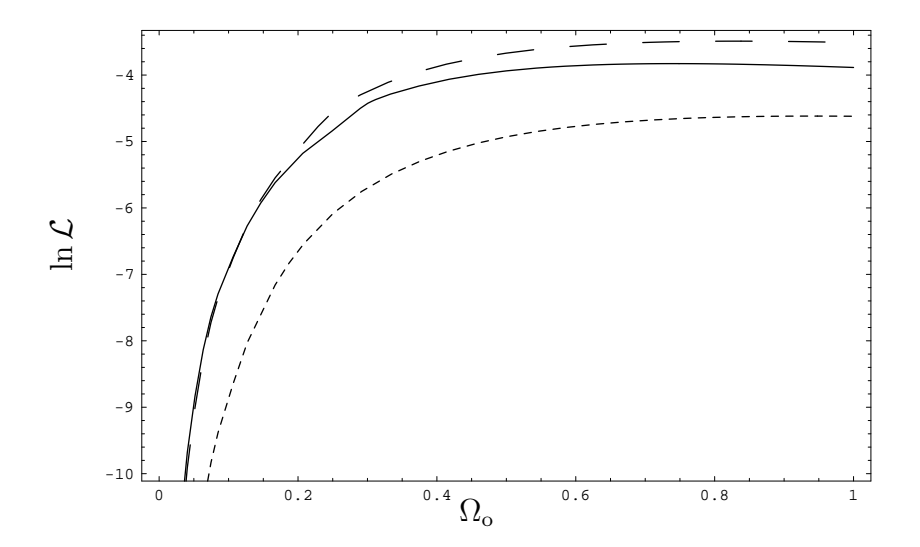


Figure 6: Plots of likelihood functions vs $\Omega_{\rm o}$. The solid curve is the plot for $r_{\rm c}^*=45~h^{-1}{\rm pc}$, $\sigma_{\rm DM}^*=203~{\rm km~s^{-1}}$, and $\gamma=2.83$ in flat universe models using only the LBQS result. The dash-dash curve represents the plot for $r_{\rm c}^*=45~h^{-1}{\rm pc}$, $\sigma_{\rm DM}^*=178~{\rm km~s^{-1}}$, and $\gamma=1.89$. The dot-dot curve is the plot for $r_{\rm c}^*=0$, $\sigma_{\rm DM}^*=203~{\rm km~s^{-1}}$, $\gamma=4$ and luminosity function parameter $\alpha=-1$.

	β	0	0.025	0.05	0.075	0.1	0.125	0.15	0.175	0.2	0.225
<	A >	4	5.81	7.08	8.44	9.99	11.9	14.1	16.9	20.4	24.9
-											
•	β		0.25	0.275	0.3	0.325	0.35	0.375	0.4	0.425	0.5
	< A	>	30.7	38.7	49.9	66.3	91.6	134	213	383	∞

Table 1: Averaged amplification as a function of β .

β	$A_{ m M}$	$L_1(A_{ m M})$	$L_{\rm o}$
0	2	1	1
0.05	4.03321	0.538516	0.580948
0.1	5.98959	0.381634	0.427036
0.15	8.71889	0.276166	0.318752
0.2	12.8853	0.19801	0.235198
0.25	19.8151	0.137874	0.168375
0.3	32.6748	0.0910677	0.114322
0.35	60.7457	0.0549151	0.0708916
0.4	141.863	0.0278588	0.037016
0.45	585.195	0.00920176	0.0126015
0.49	14931.9	0.000780135	0.001096
0.5	∞	0	0

Table 2: $A_{\rm M},\,L_1(A_{\rm M}),\,{\rm and}\,\,L_{\rm o}$ as a function of $\beta.$

NGC	$\theta_c \text{ (arcsec)}$	Distance $(h^{-1}\text{Mpc})$	$m(B_{\mathrm{T}}(0))$
720	4.58 ± 0.01	20.5 ± 4.4	11.13
741	1.91 ± 0.03	53 ± 11	12.18
1395	$1.86 {\pm} 0.12$	19.9 ± 1.9	10.52
1407	3.21 ± 0.07	19.9 ± 1.9	10.51
1600	3.73 ± 0.09	40.2 ± 4.9	11.85
3379	$1.66 {\pm} 0.07$	8.6 ± 1.3	10.17
4261	2.61 ± 0.05	27.8 ± 5.9	11.32
4365	2.33 ± 0.02	13.33 ± 0.71	10.42
4374	2.99 ± 0.02	13.33 ± 0.71	9.91
4472	3.7 ± 0.03	13.33 ± 0.71	9.26
4636	3.24 ± 0.17	13.33 ± 0.71	10.37
4649	$3.41 {\pm} 0.11$	13.33 ± 0.71	9.7
5846	2.51 ± 0.14	23.4 ± 2.8	10.87

Table 3: Core radii of sample galaxies and their corresponding distances and apparent magnitudes.

Source	z_s	z_l	m_l	$\Delta\theta$ (arcsec)
Q0142-100	2.719	0.49	$R \approx 19$	2".2
PG1115+080	1.722	0.294	$R \approx 19.8$	2".3
H1413 + 117	2.551	$1.4382^a \ (1.6603^a)$		1″23
LBQS1009-0252	2.739	0.869^{a}	R > 21	1."53
Q1208+1011	3.803	$1.1349^a \ (2.9157^a)$		0".45

^a The assumed galaxy redshifts, based on the most possible absorption lines by observers in literature.

Table 4: Parameters of gravitational lensing systems. First column: the name of each quasar in each lensing system. Second column: the source redshift. Third column: the lens redshift. Fourth column: the apparent magnitude (in R band) of each galaxy, if the value is available. Fifth column: the angular splitting of each lensing system. We take the average separation value of the quadruple system H1413+117.

	$\Omega_{\rm o}$ =	$=0, \Omega_{\Lambda}=1$		$\Omega_{\rm o} = 0$	$\Omega_{\Lambda}=0.8$	
source	$\sigma_{\rm DM}({\rm km~s^{-1}})$	$r_{\rm c}(h^{-1}{\rm pc})$	$B_{T}(0)$	$\sigma_{\rm DM}({\rm km~s^{-1}})$	$r_{\rm c}(h^{-1}{\rm pc})$	$B_{T}(0)$
Q0142-100	217	62	21.8	233	86	21.4
PG1115+080	221	67	20.4	230	81	20.1
H1413+117	223	69	25.2	275	185	23.9
$H1413 + 117^a$	250	119	25.3	324	398	23.8
LBQS1009-0252	198	40	23.9	224	72	23.1
Q1208+1011	106	2.1	26.7	124	4.5	25.7
^a Galaxy redshift	is 1.66.					

Table 5: Theoretical predictions of velocity dispersions, core radii, and apparent magnitudes of lenses in flat universe models. K-correction is not included in the fourth and seventh columns. We choose $\sigma_{\rm DM}^* = 203~{\rm km~s^{-1}}$, $r_{\rm c}^* = 45h^{-1}$ pc, and $\gamma = 2.83$.

	$\Omega_{\rm o} =$	$=0, \Omega_{\rm R}=1$		$\Omega_{\rm o} = 0.2$	$25, \Omega_{\rm R} = 0.75$	
source	$\sigma_{\rm DM}({\rm km~s^{-1}})$	$r_{\rm c}(h^{-1}{\rm pc})$	$B_{T}(0)$	$\sigma_{\rm DM} ({\rm km~s^{-1}})$	$r_{\rm c}(h^{-1}{\rm pc})$	$B_{T}(0)$
Q0142-100	254	129	21.0	254	127	20.9
PG1115+080	244	107	19.8	244	107	19.8
H1413 + 117	316	354	23.3	320	376	23.1
$H1413 + 117^a$	390	954	23.1	420	1338	22.7
LBQS1009-0252	252	123	22.5	251	122	22.4
Q1208+1011	141	8.3	25.1	140	8.0	24.9
^a Galaxy redshift	is 1.66.					

Table 6: Theoretical predictions of velocity dispersions, core radii, and apparent magnitudes of lenses in open universe models. K-correction is not included in the fourth and seventh columns. We choose $\sigma_{\rm DM}^*=203~{\rm km~s^{-1}},\,r_{\rm c}^*=45h^{-1}$ pc, and $\gamma=2.83$.

$\Omega_{\rm o}$	$N_{\rm exp}^{a,b}$	$\ln \mathcal{L}^{a,b}$	$N_{\rm exp}^{a,c}$	$\ln \mathcal{L}^{a,c}$	$N_{\mathrm{exp}}^{a,d}$	$\ln \mathcal{L}^{a,d}$	$N_{\mathrm{exp}}^{b,e}$	$\ln \mathcal{L}^{b,e}$	$N_{\rm exp}^{c,e}$	$\ln \mathcal{L}^{c,e}$	$N_{\mathrm{exp}}^{e,f}$	$\ln \mathcal{L}^{e,f}$	$N_{\rm exp}^{c,g}$	$\ln \mathcal{L}^{c,g}$	$\ln \mathcal{L}^{c,g,h}$
0	21.0	-28.16	22.2	-27.95	47.7	-54.69	14.7	-14.91	15.5	-15.49	19.5	-19.16	16.1	-20.63	-20.73
0.05	10.8	-19.93	11.3	-18.98	24.8	-33.43	8.3	-8.95	8.8	-9.13	11.3	-11.53	7.7	-15.37	-15.75
0.1	7.5	-18.11	7.9	-16.86	17.4	-27.25	6.0	-6.92	6.3	-6.95	8.3	-8.88	5.2	-14.57	-15.12
0.15	5.8	-17.56	6.1	-16.11	13.5	-24.30	4.7	-5.87	5.0	-5.81	6.6	-7.50	4.0	-14.55	-15.20
0.2	4.7	-17.47	4.9	-15.87	11.0	-22.63	3.9	-5.24	4.1	-5.13	5.4	-6.65	3.2	-14.78	-15.52
0.25	3.9	-17.59	4.1	-15.80	9.3	-21.63	3.3	-4.83	3.5	-4.56	4.7	-6.09	2.7	-15.04	-15.85
0.3	3.4	-17.74	3.6	-15.93	8.0	-20.99	2.9	-4.43	3.0	-4.25	4.1	-5.70	2.3	-15.43	-16.29
0.35	3.0	-18.03	3.1	-16.12	7.1	-20.59	2.5	-4.24	2.6	-4.03	3.6	-5.41	2.0	-15.84	-16.75
0.4	2.6	-18.36	2.8	-16.36	6.3	-20.34	2.3	-4.10	2.4	-3.87	3.2	-5.20	1.7	-16.25	-17.22
0.45	2.4	-18.70	2.5	-16.61	5.7	-20.10	2.0	-4.01	2.1	-3.76	2.9	-5.05	1.6	-16.67	-17.68
0.5	2.1	-19.04	2.2	-16.88	5.1	-20.03	1.8	-3.94	1.9	-3.67	2.7	-4.93	1.4	-17.08	-18.14
0.55	2.0	-19.39	2.0	-17.16	4.7	-20.02	1.7	-3.89	1.8	-3.61	2.5	-4.84	1.3	-17.50	-18.60
0.6	1.8	-19.74	1.9	-17.43	4.3	-20.04	1.6	-3.86	1.6	-3.56	2.3	-4.77	1.2	-17.92	-19.06
0.65	1.7	-20.08	1.7	-17.70	4.0	-20.09	1.4	-3.84	1.5	-3.53	2.1	-4.72	1.1	-18.35	-19.52
0.7	1.5	-20.42	1.6	-17.98	3.7	-20.16	1.3	-3.83	1.4	-3.51	2.0	-4.68	1.0	-18.78	-19.99
0.75	1.4	-20.76	1.5	-18.24	3.5	-20.25	1.3	-3.83	1.3	-3.50	1.8	-4.66	0.9	-19.22	-20.48
0.8	1.3	-21.09	1.4	-18.51	3.2	-20.35	1.2	-3.83	1.2	-3.49	1.7	-4.64	0.9	-19.70	-20.99
0.85	1.2	-21.42	1.3	-18.76	3.0	-20.46	1.1	-3.84	1.1	-3.49	1.6	-4.63	0.8	-20.22	-21.54
0.9	1.2	-21.74	1.2	-19.02	2.9	-20.58	1.0	-3.85	1.1	-3.49	1.5	-4.62	0.7	-20.85	-22.21
0.95	1.1	-22.05	1.1	-19.26	2.7	-20.71	1.0	-3.87	1.0	-3.50	1.5	-4.62	0.7	N/A	N/A
1.	1.0	-22.36	1.1	-19.51	2.6	-20.84	0.9	-3.89	1.0	-3.51	1.4	-4.62	0.7	N/A	N/A

^a All five quasar surveys and lensing events are used.

Table 7: Expected lensing events and likelihood analysis. This table is for flat universe models, i.e., $\Omega_{\rm o} + \Omega_{\Lambda} = 1$. $N_{\rm exp}$ is our theoretical prediction of the number of lensing events, and $\ln \mathcal{L}$ is the logarithm of the maximum likelihood function. $z_l = 1.438$ in system H1413+117 and $z_l = 1.1349$ in system Q1208+1011 are generally used, unless otherwise noted.

 $[^]b$ $\sigma_{\rm DM}^* = 203~{\rm km~s^{-1}},\, r_{\rm c}^* = 45 h^{-1}$ pc, and $\gamma = 2.83.$

 $^{^{}c}$ $\sigma_{\rm DM}^{\rm *}=178~{\rm km~s^{-1}},~r_{\rm c}^{*}=45h^{-1}~{\rm pc,~and}~\gamma=1.89.$ d $\sigma_{\rm DM}^{*}=207~{\rm km~s^{-1}},~r_{\rm c}^{*}=28h^{-1}~{\rm pc,~and}~\gamma=1.89.$

^e Only LBQS and LBQS1009-0252 are considered.

 $f \sigma_{\rm DM}^* = 225 \text{ km s}^{-1}, r_{\rm c}^* = 0, \gamma = 4, \text{ and } \alpha = -1.$

^g Based on surveys by Crampton et al. [30], Maoz et al. [29], Surdej et al. [31], and Yee et al. [32]. Four lensing events are used. $z_l = 2.9157$ in system Q1208+1011 is used. There is

no solution for r_c and $\sigma_{\rm DM}$ of the system Q1208+1011 when $\Omega_{\rm o} \geq 0.95$.

 $^{^{}h}$ $z_{l} = 1.66$ in system H1413+117.

$\Omega_{\rm o}$	$N_{\rm exp}^{a,b}$	$\ln \mathcal{L}^{a,b}$	$N_{\rm exp}^{a,c}$	$\ln \mathcal{L}^{a,c}$	$N_{\rm exp}^d$	$\ln \mathcal{L}^d$	$\ln \mathcal{L}^{d,e}$
0	2.1	-19.43	5.0	-22.34	1.3	-16.04	-16.99
0.05	1.9	-19.61	4.7	-22.38	1.3	-16.40	-17.39
0.1	1.9	-19.79	4.5	-22.43	1.2	-16.74	-17.76
0.15	1.8	-19.96	4.3	-22.49	1.2	-17.06	-18.12
0.2	1.7	-20.06	4.1	-22.49	1.1	-17.29	-18.38
0.25	1.6	-20.23	4.0	-22.56	1.1	-17.59	-18.70
0.3	1.6	-20.39	3.8	-22.64	1.0	-17.87	-19.01
0.35	1.5	-20.55	3.7	-22.72	1.0	-18.14	-19.31
0.4	1.5	-20.70	3.6	-22.80	0.9	-18.41	-19.61
0.45	1.4	-20.86	3.5	-22.89	0.9	-18.68	-19.89
0.5	1.4	-21.01	3.3	-22.98	0.9	-18.94	-20.18
0.55	1.3	-21.15	3.2	-23.07	0.9	-19.21	-20.47
0.6	1.3	-21.30	3.2	-23.16	0.8	-19.48	-20.76
0.65	1.3	-21.44	3.1	-23.25	0.8	-19.75	-21.06
0.7	1.2	-21.58	3.0	-23.34	0.8	-20.04	-21.36
0.75	1.2	-21.71	2.9	-23.43	0.8	-20.35	-21.69
0.8	1.2	-21.85	2.8	-23.52	0.7	-20.69	-22.06
0.85	1.1	-21.98	2.8	-23.61	0.7	-21.11	-22.49
0.9	1.1	-22.11	2.7	-23.70	0.7	-21.79	-23.18
0.95	1.1	-22.24	2.6	-23.79	0.7	N/A	N/A
1.	1.0	-22.36	2.6	-23.88	0.7	N/A	N/A

^a All five quasar surveys and lensing events are used.

Table 8: Expected lensing events and likelihood analysis. This table is for open universe models, i.e., $\Omega_{\Lambda} = 0$. $N_{\rm exp}$ is our theoretical prediction for the number of lensing events, and $\ln \mathcal{L}$ is the logarithm of the maximum likelihood function. $z_l = 1.438$ in system H1413+117 and $z_l = 1.1349$ in system Q1208+1011 are generally used, unless otherwise noted.

 $^{^{}b}$ $\sigma_{\rm DM}^{*}=203~{\rm km~s^{-1}},~r_{\rm c}^{*}=45h^{-1}~{\rm pc},~{\rm and}~\gamma=2.83.$ c $\sigma_{\rm DM}^{*}=207~{\rm km~s^{-1}},~r_{\rm c}^{*}=28h^{-1}~{\rm pc},~{\rm and}~\gamma=1.89.$ d $\sigma_{\rm DM}^{*}=178~{\rm km~s^{-1}},~r_{\rm c}^{*}=45h^{-1}~{\rm pc},~{\rm and}~\gamma=1.89.$ Based on surveys by Crampton et al. [30], Maoz et al. [29], Surdej et al. [31], and Yee et al. [32]. Four lensing events are used. $z_l = 2.9157$ in system Q1208+1011 is used. There is no solution for r_c and $\sigma_{\rm DM}$ of the system Q1208+1011 when $\Omega_o \geq 0.95$.

 $^{^{}e}$ $z_{l} = 1.66$ in system H1413+117.